ELSEVIER

Thermochimica Acta 329 (1999) 129–139

thermochimica acta

Synthesis, characterization and thermal decomposition kinetics of barium(II)-bis(oxalato)barium(II)dihydrate and lead(II)bis(oxalato)lead(II)monohydrate

N. Deb[a,*], S.D. Baruah[b], N. Sen Sarma[c], N.N. Dass[c]

[a]*Department of Chemistry, North Eastern Regional Institute of Science and Technology, Nirjuli 791 109, Arunachal Pradesh, India*
[b]*Regional Research Laboratory, Jorhat 785 006, Assam, India*
[c]*Department of Chemistry, Dibrugarh University, Dibrugarh 786 004, Assam, India*

Received 19 June 1997; received in revised form 26 September 1998; accepted 15 January 1999

Abstract

Barium(II)bis(oxalato)barium(II)dihydrate (BOD), $Ba[Ba(C_2O_4)_2]\cdot 2H_2O$ and lead(II)bis(oxalato)lead(II)monohydrate (LOM), $Pb[Pb(C_2O_4)_2]\cdot H_2O$ have been synthesized and characterized by elemental analysis, conductance measurements, IR spectral, reflectance and X-ray powder diffraction studies. Thermal decomposition studies (TG, DTG and DTA) in air showed that at ca. 1000°C, a mixture of BaO_2 and $BaCO_3$ is generated from the compound, BOD, through the formation of BaO_2 and BaC_2O_4 at around 514°C as intermediates. LOM gave Pb_2O_3 as final product at ca. 390°C. DSC study in nitrogen showed a different decomposition pattern from that in air for both compounds. Using seven mechanistic equations, the rate controlling process of the dehydration and decomposition mechanism of BOD is inferred to be one- and three-dimensional diffusion, respectively. The decomposition mechanism of LOM is a phase boundary reaction having cylindrical symmetry. Some of the decomposition products were identified by analytical, IR spectral and X-ray powder diffraction studies. A tentative reaction mechanism for the thermal decomposition of both the complexes is proposed.

Keywords: Synthesis; Characterization; Oxalato; Thermal decomposition; Kinetics

1. Introduction

The chemistry of metal oxalato complexes of both simple and complex types are classified and reviewed by Krishnamurty and Harris [1]. Transition and non-transition metal oxalates of different types have been extensively studied by many workers [2–6]. The structure of $BaC_2O_4\cdot H_2O$ was confirmed [7] by X-ray diffraction which led to $BaCO_3$ and CO at around 395°C in N_2 atmosphere, whereas Fabbri and Baraldi [8] reported the formation of $BaCO_3$ at >380°C in vacuum as well as lead oxide as final product from PbC_2O_4. Further they showed [9] that both the compounds decomposed to oxide or oxide and metal. A gas chromatography study showed [10] PbO formed as end product from PbC_2O_4 via the formation of carbonate as intermediate. Usha et al. [11] suggested that the compound, $NH_4Ba[Co(C_2O_4)_3]\cdot nH_2O$ decomposes in a complex manner and the final product is influenced by the surrounding atmosphere. The oxalate of the mixed metal of barium and titanium of the type $BaTiO(C_2O_4)_2$ was reported by Gopalakhrishna-Murthy et al. [12]. The same workers [13] prepared the

*Corresponding author. Tel.: +91-360-257659; fax: +91-360-244307/+91-360-257696; e-mail: chem@nerist.ernet.in

0040-6031/99/$ – see front matter
PII: S0040-6031(99)00042-8

compound $PbTiO(C_2O_4)_2{\cdot}4H_2O$, and reported $PbTiO_3$ as the final product in air or O_2. Compounds of the type $M_2U(C_2O_4)_4{\cdot}nH_2O$ (where M=Ba, Pb, Ca, Cd, Sr) have been reported [14]. A mossbauer study [15] of the thermal decomposition of $Ba_3[Fe(C_2O_4)_3]{\cdot}nH_2O$ led to $BaFe^{III}O_4$ at higher temperatures. Recently, Dollimore [16] reviewed oxalato compounds and emphasized [17] the dependence of the thermal stability of oxalate on the environmental atmosphere, sample preparation and prehistory. Mechanistic equations are used [18–20] to study the kinetics and mechanism of the thermal decomposition. In continuation of our work [21–31] on the compounds of the type $M[M(C_2O_4)_2]{\cdot}xH_2O$ (where M=same metal), we are reporting here the synthesis, characterization and thermal decomposition of $Ba[Ba(C_2O_4)_2]{\cdot}2H_2O$ (BOD) and $Pb[Pb(C_2O_4)_2]{\cdot}2H_2O$ (LOM) in air and nitrogen media. Mechanism of the decomposition have been investigated on the basis of different mechanistic equations. The tentative mechanism for the decomposition in air has also been proposed.

2. Experimental

The compounds were prepared by the method described [22–31] earlier from the respective metal chlorides. The compounds were purified by standard procedures and were air dried at ambient temperature and stored in a desiccator. Water and metal contents were determined thermogravimetrically and gravimetrically by known methods. Carbon and hydrogen were analyzed using Carlo Erba 1108 elemental analyzer.

The IR spectra were measured from 200 to 4000 cm^{-1} in nujol mulls with a Perkin-Elmer 883 spectrophotometer. IR spectra of the gases evolved during decomposition were recorded by the reported [21] method. Diffuse reflectance spectra were recorded with a Shimadzu UV-240 spectrophotometer using $BaSO_4$ as the reference material.

TG, DTG and DTA of lead compounds were recorded in static air at a heating rate of 10°C min^{-1} using a Shimadzu DT 30B thermal analyzer. The amount of sample taken was 15.48 mg. For barium compound CHAN (USA), DTA and TGA units (model 131) were used to carry out the thermal study. The furnace atmosphere was static air. The heating rate and sample mass were 10°C min^{-1} and 28.25 mg, respectively. DSC curves were recorded up to 670°C using Perkin Elmer DSC-7 at a heating rate of 10°C min^{-1} in nitrogen atmosphere. The kinetic parameters of the phase transformation process were determined.

The electrical conductivity of the compounds were measured at 1 kHz with the help of Aplab (India) LCR-Q meter (model no. 4910). The powder samples were pressed at 3.73×10^9 kg m^{-2} to make pellets and the graphite paint was used as electrode. The X-ray powder diffraction pattern of the compounds and the decomposition products were taken using a Geigerflex Microprocessor controlled Automated Rigaku (Japan) X-ray diffractometer system D/Max IIIC. Sometimes the model JDX-11P3A JEOL diffractometer using Ni filter with Cu K_α radiation at 35 kV and 10 mA in the wide angle $2^\circ<2\theta<60^\circ$ was also used to take the XRD pattern of the powder sample.

3. Theoretical

Evaluation of the mechanism of reaction using mechanistic equations has been discussed by several authors [18–20]. We have used the following kinetic expression [20]:

$$\frac{\Delta \ln \alpha'}{\Delta \ln(1-\alpha)} = -\frac{E^*}{R}\frac{\Delta(1/T)}{\Delta \ln(1-\alpha)} + \frac{\Delta \ln f(\alpha)}{\Delta \ln(1-\alpha)}, \quad (1)$$

where the terms have their usual meaning and $f(\alpha)$ is a function depending on the actual mechanism of the process. A series of seven forms of $f(\alpha)$ are proposed in [20] out of the possible mechanisms [19] of thermal decomposition. Thus a plot of $\Delta \ln \alpha' - \Delta \ln f(\alpha)/\Delta \ln(1-\alpha)$ against $\Delta(1/T)/\Delta \ln(1-\alpha)$ is a straight line whose slope is $-E^*/R$, irrespective of the form of $f(\alpha)$ employed. One can select the $f(\alpha)$ that best fits the actual mechanism of reaction corresponding to the intercept value close to zero.

Further, to test the correctness and validity of the above conclusion regarding the identification of the actual mechanism of the process, the Arrhenius equation of the following type [20] is used.

$$\ln \alpha' - \ln f(\alpha) = \ln(A/\beta) - E^*/RT, \quad (2)$$

where the terms have their usual meaning. The slope, $-E^*/R$, and intercept, $\ln(A/\beta)$, can be obtained from the plot of $\ln \alpha' - \ln f(\alpha)$ against $1/T$ which is a straight line. It now follows that the mechanism proposed on the basis of the kinetic Eq. (1) is correct provided the E^* value obtained from the above plot of (2) turns out to be the same.

Thus, we have evaluated the E^* from TG curves employing the kinetic Eqs. (1) and (2) for seven forms of $f(\alpha)$ and thus inferred the rate controlling process [20] for the dehydration and decomposition steps of BOD and the only decomposition step of LOM as described above. The details of the kinetic parameters calculated can be seen from Table 3.

4. Results and discussion

4.1. Characterization of complexes

The complexes $Ba[Ba(C_2O_4)_2]\cdot 2H_2O$ (BOD) and $Pb[Pb(C_2O_4)_2]\cdot H_2O$ (LOM) were isolated as white powders and were insoluble in water and common organic solvents, but decomposed in the presence of strong acid or alkali.

Water analysis, microanalytical and thermogravimetric results as well as estimated metal contents suggested the proposed formula of the compound of barium and lead, which contains two and one molecule of water, respectively. The electrical conductivity were measured to be 2.67×10^{-4} and $1.02\times10^{-7}\ \Omega^{-1}\,cm^{-1}$ for barium and lead compounds, respectively. No appreciable change has occurred in the value of conductivity of lead compound in relatively more humid atmosphere which is measured to be $4.86\times10^{-7}\ \Omega^{-1}\,cm^{-1}$. Selected bands (Table 1) in the IR spectra of the compounds suggested [29–32] the chelating character of the oxalato group. The electronic spectrum of the solid sample of BOD showed that the bands around 20 000, 23 800 (small), 26 730 and 38 900 cm^{-1} are due to L→M or M→L charge-transfer and intraligand $\pi\rightarrow\pi^*$ transitions. Similar bands observed at 20 000 and 27 390 cm^{-1} are due to $\pi\rightarrow\pi^*$ transitions for LOM, whereas intense band at 33 112 cm^{-1} could be possibly due to transition involving the Pb–Pb bond [22,33]. X-ray powder diffraction (XRD) pattern (Table 2) of BOD and LOM are, however, different from each other which suggests that they are not isomorphous.

4.2. Decomposition of the complexes

The TG curve (Fig. 1) of $Ba[Ba(C_2O_4)_2]\cdot 2H_2O$ (BOD) showed that the mass loss was started around 110°C and an inclined slope up to 170°C with mass loss of 5.5% (calculated, 5.55%) indicated the removal of one and a half molecules of water. DTG change

Table 1
Selected bands in the IR spectra of $Ba[Ba(C_2O_4)_2]\cdot 2H_2O$ (BOD) and $Pb[Pb(C_2O_4)_2]\cdot H_2O$ (LOM)

IR bands[a] (cm^{-1})		Assignments
BOD	LOM	
2400–3840b (split into 2960, 3280, 3340, 3560)	–	ν_{sy}(O–H)+ν_{asy}(O–H) or hydrogen bonding
1640s	1600sb	δ_{sy}(O–H–O)
1480–1760b (split into 1660s, 1600s, 1560s)	1400–1700b	ν_{asy}(C=O)
~1395 small, 1475s	1370 small	ν_{sy}(C–O) and/or ν(C–C)
1320s	~1320m, ~1295sm	ν_{sy}(C–O)and/or δ(O–C=O)
850s, 880sh	–	ν_{sy}(C–O) and/or δ(O–C=O)
~750, ~770m, ~790m	~790 (split into 780)	ν(M–O) and/or δ(O–C=O) or co-ordinated water
600m	~600 small	Water of crystallization
540m	–	ν(M–O) and/or ν(C–C)
480m, 450sh	485, 470 (split)	δ(O–C=O) and/or ring deformation
395m	380m	δ(O–C=O)
350m	360m	δ(O–C=O) and/or ν(C–C)
–	294 small	π (out-of-plane bending)

[a] b=broad; m=medium; s=strong and sh=shoulder.

Table 2
Prominent lines in the X-ray powder diffraction pattern of $Ba[Ba(C_2O_4)_2]\cdot 2H_2O$ (BOD) and $Pb[Pb(C_2O_4)_2]\cdot H_2O$ (LOM)

$Ba[Ba(C_2O_4)_2]\cdot 2H_2O$		$Pb[Pb(C_2O_4)_2]\cdot H_2O$	
d (Å)	I/I_0 (Rel)	d (Å)	I (Rel)
6.538	85	7.369	4.72
6.197	83	6.321	3.60
5.719	100	6.188	2.34
5.542	74	5.981	3.64
5.375	69	5.604	3.28
5.218	68	5.434	3.48
5.056	66	5.273	1.31
4.877	92	4.951	22.16
4.685	69	4.741	17.59
4.420	66	4.480	10.71
4.079	52	4.288	20.40
3.529	56	4.149	7.16
3.403	58	4.001	100.00
3.177	41	3.783	3.33
3.055	47	3.720	1.50
2.942	73	3.573	5.29
2.855	36	3.490	1.44
2.790	44	3.411	6.54
2.748	66	3.229	2.10
2.688	39	3.140	2.57
2.523	36	3.097	1.96
2.486	31	2.996	1.21
2.456	31	2.486	1.69
2.434	29	2.220	1.21
2.384	42	2.174	1.67
2.363	50	2.102	1.70
2.079	59	2.004	1.30
2.011	44		
1.962	27		
1.950	33		
1.860	23		
1.628	23		

(112–180°C) and an endotherm between 140°C and 210°C (ΔT_{min}=186°C) in DTA correspond to the dehydration step. The inclined nature of the TG curve has changed nearly to flat with two minor breaks at 205°C and 238°C which may be accounted for the elimination of remaining traces of water. Two small peaks at 205°C and 235°C are distinct in DTG curve. The complete deaquated species is assumed to be around 325°C in TG (mass loss, found, 7.5%; calculated, 7.39%) and is stable upto 450°C. The activation energy (E^*) of this step was calculated (Table 3) using mechanistic equations. The rate controlling process of deaquation is found to be one-dimensional diffusion. The study suggested that the dehydration had taken place with lower activation energy in most of the mechanisms. In the first two processes the E^* are more than double of other mechanisms. In DSC in nitrogen a strong endothermal change is observed for dehydration between 137.3°C and 172°C and the kinetic parameters are recorded in Table 4. The XRD data of the calcined residue in furnace at 300°C are included in Table 5. Most of the d values are similar to the parent compound. The mass loss started in case of $BaC_2O_4\cdot H_2O$ [7] was 97°C.

Decomposition of the anhydrous species started from 450°C and a steep slope in TG up to 514°C apparently indicates that the product might be a mixture of BaO_2 and BaC_2O_4 (mass loss, found, 18.5%; calculated, 18.94%). This type of species is anticipated earlier [27,28,31]. Pyrolysed compound at 330°C (mass loss, 17.5%) in furnace is grayish white in color. The chemical and IR spectral studies of the separated compounds suggest that the species might be BaC_2O_4 and barium oxide. The trace amount of CO(g) and CO_2(g) evolved were detected by their IR study and the band position were in conformity with the works reported elsewhere [31,32]. Interestingly, the mass loss occurs very slowly after 514°C in TG with two small breaks at 800°C (21.4% mass loss) and 886°C (22.5% mass loss) which might be ascribed to the conversion of BaO_2 to BaO. The theoretical mass loss to get BaO and BaC_2O_4 from the parent compound is 22.23%. The reduction of BaO_2 to BaO by CO(g) evolved during rupture of $C_2O_4^{2-}$ group cannot be neglected. This type of conversion by heating in air is also possible. Hence, the two small breaks in TG curve might be responsible for the above changes. Two small peaks appear at 800°C and 850°C in DTA profile after a strong exothermic peak between 450°C and 530°C (ΔT_{max}=515°C) which is due to main decomposition phase are in good agreement with the TG changes and the presumed phenomena. DTG change between 450°C and 530°C for the main decomposition followed by two small changes at 800°C and 890°C are accounted for by the subsequent changes of the product. The decomposition of BaC_2O_4 starts at about 395°C as reported by Nagase et al. [7], whereas in this study the stability of the intermediate BaC_2O_4 is enhanced due to the influence of BaO, like CaO on CaC_2O_4 [31]. After the small inflexion in TG at 886°C, the mass loss continued slowly and finally 24.5% mass loss at 1000°C indicates that the product may be a

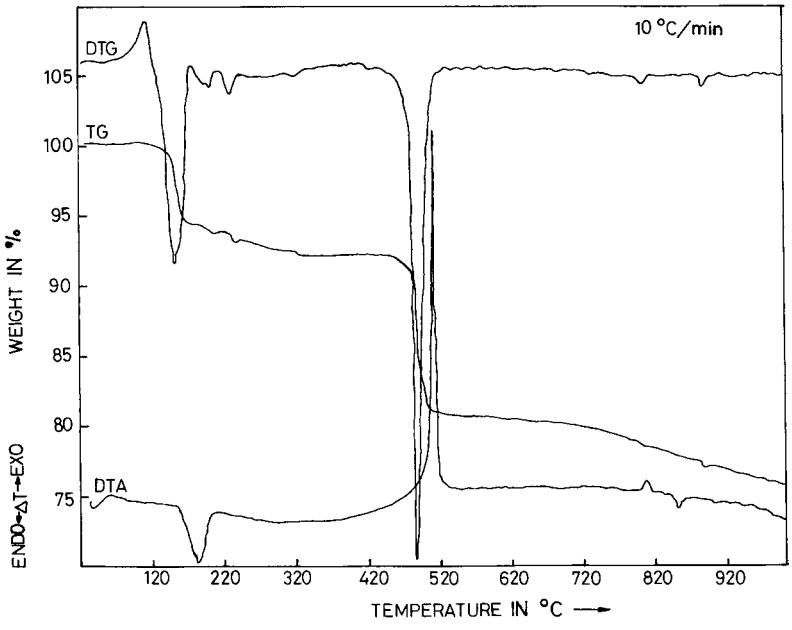

Fig. 1. TG, DTG and DTA curves of $Ba[Ba(C_2O_4)_2]\cdot 2H_2O$ at 10°C min^{-1} in air.

Table 3
Kinetic data evaluated by the seven mechanistic equations

Compound	Step	Mechanism	(A)		(B)		Difference of E^* between (A) and (B) (%)
			Correlation coefficient (r)	E^* (kJ mol^{-1})	E^* (kJ mol^{-1})	A (s^{-1})	
BOD	Dehydration	D1	0.9989	237.53	237.53	1.06×10^{27}	00.00
		D2	0.9865	244.51	301.37	2.33×10^{34}	18.86
		D3	0.9953	90.92	99.75	4.78×10^{12}	8.85
		D4	0.9899	95.23	110.83	1.25×10^{13}	14.08
		F1	0.9847	83.14	109.12	5.19×10^{12}	23.81
		R2	0.9868	93.85	114.31	1.12×10^{13}	17.89
		R3	0.9976	93.51	92.34	1.66×10^{10}	1.25
	Decomposition	D1	0.9166	346.39	415.68	2.95×10^{26}	16.67
		D2	0.9793	389.69	445.39	1.69×10^{28}	12.50
		D3	0.9972	113.36	113.37	3.01×10^{7}	00.00
		D4	0.8784	191.84	249.41	6.46×10^{15}	23.08
		F1	0.9276	311.74	415.68	1.02×10^{27}	25.00
		R2	0.9372	283.38	415.68	4.89×10^{26}	31.83
		R3	0.9012	249.41	311.75	3.09×10^{19}	19.99
LOM	Decomposition	D1	0.9987	508.06	623.54	1.01×10^{49}	18.52
		D2	0.9928	531.16	669.69	2.82×10^{52}	20.69
		D3	0.8963	115.44	170.87	1.64×10^{16}	32.44
		D4	0.9982	207.86	323.29	2.69×10^{25}	35.71
		F1	0.9620	254.01	323.29	2.24×10^{25}	21.43
		R2	0.9989	300.20	300.20	1.41×10^{23}	00.00
		R3	0.9212	207.86	277.11	1.32×10^{21}	24.98

(A) Results obtained by using the seven mechanisms for the plot of $(\Delta \ln \alpha' - \Delta \ln f(\alpha)/\Delta \ln(1-\alpha))$ vs. $\Delta(1/T)/\Delta \ln(1-\alpha)$, and (B) for the Arrhenius plot of $\ln \alpha'/f(\alpha)$ vs. $1/T$, for $Ba[Ba(C_2O_4)_2]\cdot 2H_2O$ (BOD) and $Pb[Pb(C_2O_4)_2]\cdot H_2O$ (LOM).

Table 4
DSC data of $Ba[Ba(C_2O_4)_2]\cdot 2H_2O$ (BOD) and $Pb[Pb(C_2O_4)_2]\cdot H_2O$ (LOM) in nitrogen at a heating rate of 10°C min^{-1}

Compound	Step	Temperature range (°C)	Peak temperature (°C)	$\ln k_0$ (s^{-1})	E^* (kJ mol^{-1})	ΔH (kJ mol^{-1})	ΔS^* (J K^{-1} mol^{-1})	Heat of fusion (kJ mol^{-1})	Order of reaction	Reaction
BOD	1	137.3–172 (endo)	157.4	108.8±2.4	400.3±8.6	101.8	236.6	138.9	1.38±0.02	Dehydration
	2	490.3–537.8 (endo)	515.7	102.0±2.2	697.6±15.1	21.7	27.5	31.1	1.17±0.02	Decomposition
	3	538.5–547	542.7	427.3±9.2	2916.4±63.0	0.56	0.69		1.12±0.02	
LOM	1	358.0–424.0	394.0	88.68±1.91	514.2±11.1	203.1	304.5	282.3	1.34±0.02	Decomposition

Table 5
Prominent lines with *d*-spacing and intensity of the pyrolysed product at 300°C and 700°C of $Ba[Ba(C_2O_4)_2]\cdot 2H_2O$ (BOD) and at 650°C of $Pb[Pb(C_2O_4)_2]\cdot H_2O$ (LOM)

Product at 300°C of BOD		Product at 700°C of BOD		Product at 650°C of LOM	
d (Å)	I/I_0 (Rel)	*d* (Å)	I/I_0 (Rel)	*d* (Å)	I/I_0 (Rel)
4.850	100	8.350	35	8.984	34
4.625	77	7.800	34	5.988	25
3.748	62	7.170	34	4.051	16
3.679	66	4.566	24	3.075	100
2.985	46	3.725	60	2.956	35
2.369	56	3.665	35	2.752	36
2.291	37	3.228	18	2.509	12
2.088	28	3.034	19	2.381	22
1.950	32	2.946	15	2.205	12
		2.634	23	2.011	21
		2.590	19	1.853	22
		2.294	13	1.800	19
		2.152	22	1.726	25
		2.100	13	1.643	24
		2.048	14		
		2.020	17		
		1.948	14		
		1.917	10		
		1.677	9		

mixture of BaO_2 and $BaCO_3$ (calculated, 24.69%). The oxidation of BaO again to BaO_2 could therefore be assumed. An endotherm at 850°C in DTA gives credence to this view. The TG study reveals that instead of completing the decomposition of BaC_2O_4 at around 490°C, it is generated at around 514°C which decomposes slowly to $BaCO_3$ in the presence of oxide. The formation of a trace of BaC_2 cannot be excluded from the final residue due to the interaction of BaO or molten BaO_2 with carbon formed during disproportionation of CO (g) to CO_2 (g). From the present study it can be concluded that the gray white compound at 1000°C may be a mixture of BaO/BaO_2 and $BaCO_3$ along with a trace of BaC_2. XRD pattern (Table 5) of non-separable products exhibit the peaks with *d*-values and intensities which are in close proximity with the oxide, carbonate and carbide of barium [35]. The $BaCO_3$ is found to be stable up to 1000°C in TG (indeed it decomposes to oxide at 1360°C [34]). The DSC study (Fig. 3(a)) in nitrogen shows that two overlapping endotherms from 490.3°C to 547°C is split into two peaks and their kinetic parameters are given in Table 4. Both the dehydration and decomposition steps in DSC are nearly to three-halves and first-order in kinetics, respectively. The E^* of decomposition is higher than dehydration, although it is endothermic. The mass loss of 12.93% after DSC scan suggests that the end product is a mixture of BaO and BaC_2O_4. The derived mixture might be formed through the formation of intermediate BaO_2 and BaC_2O_4 at 537.8°C and the small overlapping peak is responsible for the reduction of BaO_2 to BaO by evolved CO(g) as well as the interaction of BaO_2/BaO with carbon. The low value of enthalpy (*H*) and entropy (*S*) changes of the smaller peak suggest that the reduction and/or interaction phenomena rather than the decomposition may have occurred. The higher value of E^* corresponding to the smaller peak indicates that the possible reduction process is slow. For the main decomposition step the slope between 450°C and 514°C in TG profile is chosen for kinetic study using mechanistic equations [20]. The parameters are given in Table 2. The rate controlling process is found to be three-dimensional diffusion.

The compound, $Pb[Pb(C_2O_4)_2]\cdot H_2O$ (LOM), started to lose mass around 300°C and a steep slope in TG (Fig. 2) up to 390°C (mass loss, found, 24.3%) was observed. The product might be Pb_2O_3 (calculated, 24.03%). Corresponding to the decomposition stage in DTA exotherm between 320°C and 370°C

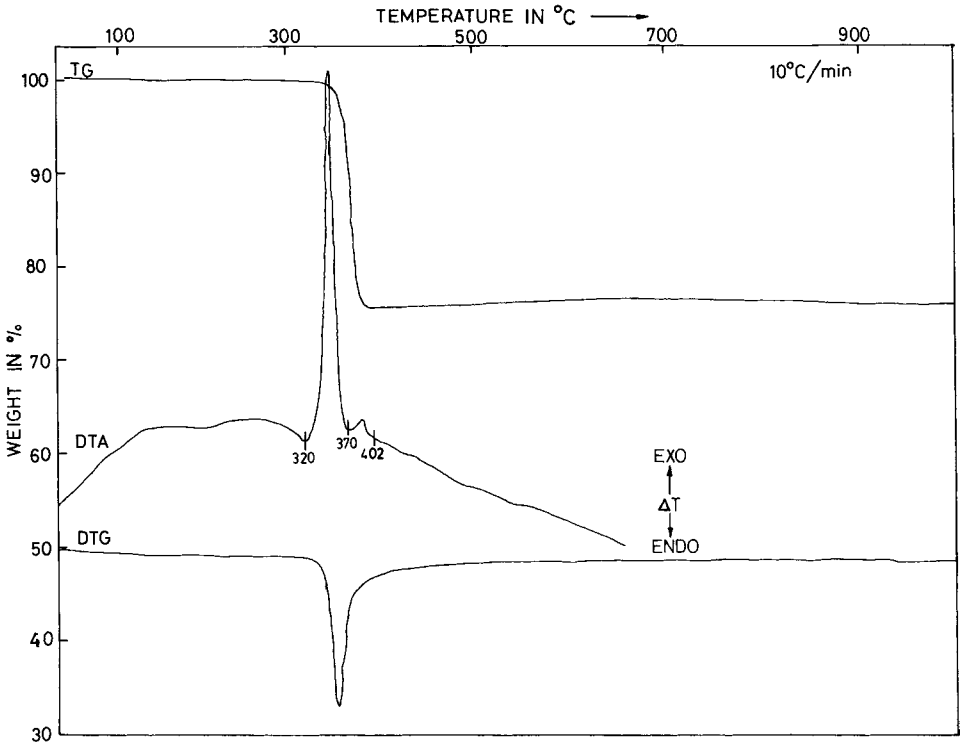

Fig. 2. TG, DTG and DTA curves of $Pb[Pb(C_2O_4)_2]\cdot H_2O$ at 10°C min^{-1} in air.

followed by a very small concomitant peak between 370°C and 402°C is recorded. DTG change between 310°C and 400°C is accounted for the corresponding changes in TG and DTA. The exothermic nature of the DTA curve from room temperature to 320°C is indicative of the formation of an intermediate species; some phase changes (or changes of crystallinity) and intramolecular rearrangement might also take place. Independent pyrolysis of the compound at 200°C in air found a species with a mass loss of 7.47%. It is assumed that the compound is a mixture of $PbCO_3$ and PbC_2O_4 (calculated, 7.59%). The compound in humid atmosphere absorbs water and might be aquated to lead oxalate. There is no indication in TG and DTG for the intermediate. However, the exothermic nature of the DTA profile from starting temperature gives credence to this view. Similar intermediates were generated earlier [30]. The removal of single water molecule at high temperature during decomposition of the complex is thought to be H-bonded with $C_2O_4^{2-}$ group and co-ordinated to Pb atom. The IR spectrum showed the same nature. As PbC_2O_4 decomposes [34] at 300°C and $PbCO_3$ at 340°C to Pb_3O_4 which behaved chemically as a mixture of PbO/PbO_2; the formation of Pb_3O_4 might also be assumed as transient intermediate in our study which immediately changes to Pb_2O_3. The XRD data (Table 5) of the calcined product around 650°C with mass loss of 24.96% confirmed [35] the residue to be Pb_2O_3. A few *d*-values are similar with the *d*-values of PbO_2 and Pb_3O_4, which suggest [35] their presence in trace along with the main product Pb_2O_3. In TG after 390°C, a slight gain of mass (0.3%) is due to partial oxidation of residue in air which is stable up to 1000°C. DTG curve shows no changes up to 1000°C. The DSC study in nitrogen (Fig. 3(b)) showed an endotherm between 358°C and 424°C. The kinetic parameters are included in Table 4. The mass loss at the end of the scan is 21.83%, which indicates the formation of $2PbO_2$ (calculated, 21.39%).

A trace of C may also be assumed in the residue due to disproportionation of CO(g) in inert medium. The decomposition follows three-halves kinetic order from

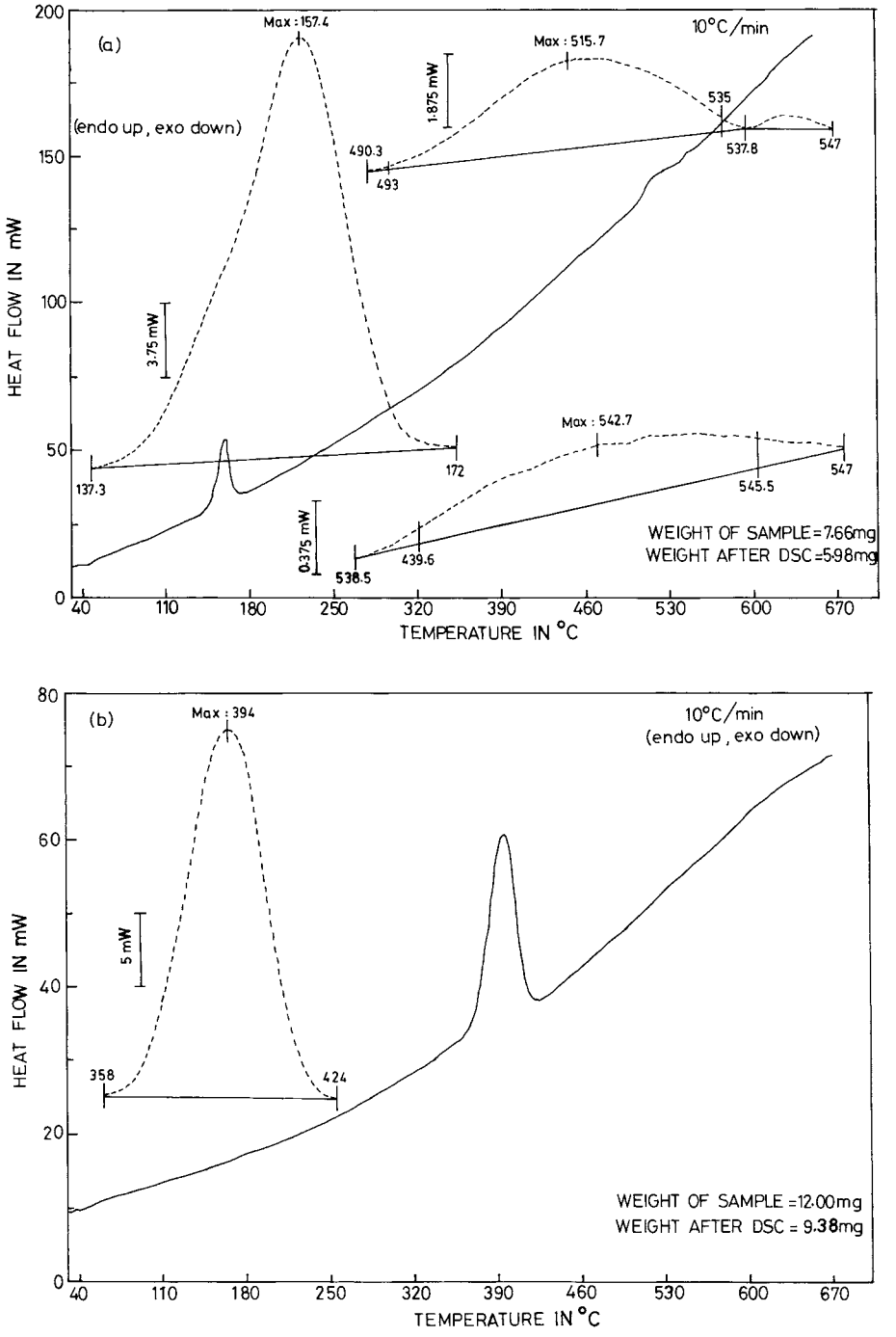

Fig. 3. DSC curves of (a) $Ba[Ba(C_2O_4)_2]\cdot 2H_2O$ and (b) $Pb[Pb(C_2O_4)_2]\cdot H_2O$ at 10°C min^{-1} in nitrogen.

DSC. From the kinetic study using mechanistic equations (Table 3), the rate controlling process of the decomposition is inferred to be a phase boundary reaction (cylindrical symmetry). Noticeable disagreements in E^* values (Table 3) were found between all the mechanistic equations and also from their Arrhenius plots. Differences are observed in the work of other authors [20].

The water vapor, carbon monoxide and carbon dioxide evolved during decomposition were identified by IR spectroscopy [31,32].

The above results suggests the following tentative scheme of the thermal decomposition in air.

In air,

$$\mathrm{Ba[Ba(C_2O_4)_2]\cdot 2H_2O} \xrightarrow{110-170^\circ\mathrm{C}} \mathrm{Ba[Ba(C_2O_4)_2]\cdot 0.5H_2O + 1.5H_2O}(v)$$

$$\xrightarrow{\text{up to } 325^\circ\mathrm{C}} \mathrm{Ba[Ba(C_2O_4)_2]}(\mathrm{s}) + 0.5\mathrm{H_2O}(v)$$

$$\xrightarrow{450-514^\circ\mathrm{C}} \mathrm{BaO_2}(\mathrm{s}) + \mathrm{BaC_2O_4}(\mathrm{s}) + \mathrm{x\,CO}(\mathrm{g})$$

$$+\mathrm{yCO_2}(\mathrm{g}) \xrightarrow[\text{continues slow decomposition}]{800-886^\circ\mathrm{C}} \mathrm{BaO}(\mathrm{s}) + \mathrm{BaC_2O_4}(\mathrm{s})$$

$$\xrightarrow{\text{ca}1000^\circ\mathrm{C}} \mathrm{BaO_2}(\mathrm{s}) + \mathrm{BaCO_3}(\mathrm{s}) + \mathrm{mCO}(\mathrm{g})$$

$$+ n\mathrm{CO_2}\,(\mathrm{g}) \xrightarrow{\text{finally}} \mathrm{BaO_2}(\mathrm{s}) + \mathrm{BaC_2}(\mathrm{s})$$

$$+\mathrm{BaCO_3}(\mathrm{s})$$

In air,

$$\mathrm{Pb[Pb(C_2O_4)_2]\cdot H_2O} \xrightarrow{\text{ca.}200^\circ\mathrm{C(pyrolysis)}} \mathrm{PbCO_3}(\mathrm{s}) + \mathrm{PbC_2O_4}(\mathrm{s})$$

$$+\mathrm{H_2O}(\mathrm{v}) + \mathrm{xCO}(\mathrm{g}) + \mathrm{yCO_2}(\mathrm{g})$$

$$\xrightarrow[\text{(transient)}]{300-390^\circ\mathrm{C}} \mathrm{Pb_3O_4}\ (\mathrm{s}) + \mathrm{mCO}(\mathrm{g}) + \mathrm{yCO_2}(\mathrm{g})$$

$$\xrightarrow[\text{(stable)}]{\text{finally}} \mathrm{Pb_2O_3}(\mathrm{s})$$

5. Conclusions

The thermal studies (TG, DTG and DTA) in air suggests that the compound BOD decomposes to peroxide, carbide and carbonate of barium around 1000°C through the formation of a mixture of barium peroxide and barium oxalate at 514°C, whereas the compound LOM produces Pb_2O_3 as the end product at ca. 390°C. The rate controlling process of the dehydration and decomposition step of BOD is inferred to be one- and three-dimensional diffusion, respectively, but in the case of LOM the decomposition mechanism is identified to be a phase boundary reaction.

References

[1] K.V. Krishnamurty, G.M. Harris, Chem. Rev. 61 (1961) 213.
[2] W.W. Wendlandt, T.D. George, K.V. Krishnamurty, J. Inorg. Nucl. Chem. 21 (1961) 69.
[3] D. Dollimore, D. Nicholson, J. Chem. Soc. (1962) 960.
[4] D. Dollimore, D.L. Griffiths, D. Nicholson, J. Chem. Soc. (1963) 2617.
[5] W.W. Wendlandt, E.L. Simmons, J. Inorg. Nucl. Chem. 28 (1966) 2420.
[6] K. Nagase, K. Sato, N. Tanaka, Bull. Chem. Soc. Jpn. 48 (1975) 868.
[7] K. Nagase, K. Sato, N. Tanaka, Bull. Chem. Soc. Jpn. 48 (1975) 439.
[8] G. Fabbri, P. Baraldi, Atti. Soc. Nat. Mat., Modena 106 (1975) 57.
[9] G. Fabbri, P. Baraldi, Atti. Soc. Nat. Mat., Modena 106 (1975) 81.
[10] T.S. Rao, B.R. Gandhi, J. Chromatogr. 88 (1974) 407.
[11] M.G. Usha, M. Subba Rao, T.R. Narayanan Kutty, J. Therm. Anal. 31 (1986) 7.
[12] H.S. Gopalakhrishna-Murthy, M. Subba Rao, T.R. Narayanan Kutty, J. Inorg. Nucl. Chem. 37 (1975) 1875.
[13] H.S. Gopalakhrishna-Murthy, M. Subba Rao, T.R. Narayanan Kutty, J. Inorg. Nucl. Chem. 38 (1976) 417.
[14] S.K. Awasthi, K.L. Chawla, D.M. Chakraburty, J. Inorg. Nucl. Chem. 36 (1974) 2521.
[15] A.S. Brar, S. Brar, S.S. Sandhu, J. Therm. Anal. 31 (1986) 1083.
[16] D. Dollimore, Anal. Chem. 66 (1994) 17R.
[17] D. Dollimore, T.A. Evans, Y.F. Lee, Thermochim. Acta 194 (1992) 215.
[18] K.N. Ninan, C.G.R. Nair, Thermochim. Acta 30 (1979) 25.
[19] W.W. Wendlandt, Thermal Methods of Analysis, Wiley, New York, 1974, p. 45.
[20] R. Lozano, J. Roman, J.C. Aviles, A. Moragues, A. Jerez, E. Ramos, Trans. Met. Chem. 12 (1987) 289.
[21] T.K. Sanyal, N.N. Dass, J. Inorg. Nucl. Chem. 42 (1980) 811.
[22] N. Deb, P.K. Gogoi, N.N. Dass, Bull. Chem. Soc. Jpn. 61 (1988) 4485.
[23] N. Deb, P.K. Gogoi, N.N. Dass, J. Ind. Council Chemists 3 (1988) 73.
[24] N. Deb, P.K. Gogoi, N.N. Dass, Thermochim. Acta 140 (1989) 145.
[25] N. Deb, P.K. Gogoi, N.N. Dass, J. Therm. Anal. 35 (1989) 27.

[26] N. Deb, P.K. Gogoi, N.N. Dass, J. Inst. Chemists (India) 61 (1989) 185.
[27] N. Deb, P.K. Gogoi, N.N. Dass, Thermochim. Acta 145 (1989) 77.
[28] N. Deb, P.K. Gogoi, N.N. Dass, J. Therm. Anal. 36 (1990) 465.
[29] N. Deb, P.K. Gogoi, N.N. Dass, Thermochim. Acta 198 (1992) 395.
[30] N. Deb, S.D. Baruah, N.N. Dass, J. Therm. Anal. 45 (1995) 457.
[31] N. Deb, S.D. Baruah, N.N. Dass, Thermochim. Acta 285 (1996) 301.
[32] K. Nakamoto, Infrared Spectra of Inorganic and Coordination Compounds, 2nd ed., Wiley/Interscience, New York, 1969, p. 83, 89, 219, 245.
[33] M.G.B. Drew, A. Lavery, V. Mckee, S.M. Nelson, J. Chem. Soc. (1985) 1771.
[34] J.A. Dean, Lange's Handbook of Chemistry, 13th ed. (Int. ed.), Mc-Graw Hill, New York, 1987, pp. 4–25, 4–27, 4–66.
[35] Inorganic Index to the Powder Diffraction File, published by Joint Committee on Powder Diffraction Standards, 1601, Parklane, Pennsylvania, 1971, p. 797, 800, 991.